This is the accepted manuscript made available via CHORUS. The article has been published as:

Probing Exciton Dispersions of Freestanding Monolayer WSe_{2} by Momentum-Resolved Electron Energy-Loss Spectroscopy

Jinhua Hong, Ryosuke Senga, Thomas Pichler, and Kazu Suenaga

Phys. Rev. Lett. **124**, 087401 — Published 25 February 2020

DOI: 10.1103/PhysRevLett.124.087401

Probing exciton dispersions of freestanding monolayer WSe_2 by momentum resolved electron energy loss spectroscopy

Jinhua Hong[1], Ryosuke Senga[1], Thomas Pichler[2], Kazu Suenaga[1,*]

[1]Nanomaterials Research Institute, National Institute of Advanced Industrial Science and Technology (AIST), Tsukuba 305-8565, Japan

[2]Faculty of Physics, University of Vienna, Strudlhofgasse 4, A-1090 Vienna, Austria

E-mail: suenaga-kazu@aist.go.jp

Excitons, as bound electron-hole paired quasiparticle, play an essential role in the energy transport in the optical/electric properties of semiconductors. Their momentum-energy dispersion relation is a fundamental physical property of great significance to understand exciton dynamics. However, this dispersion is seldom explored especially in two-dimensional transition metal dichalcogenides with rich valleytronic properties. In this work, momentum resolved electron energy-loss spectroscopy was used to measure the dispersions of excitons in free-standing monolayer WSe_2. Besides the parabolically dispersed valley excitons, a sub-gap dispersive exciton was observed at nonzero momenta for the first time, which can be introduced by the prolific Se vacancies. Our work provides a paradigm to directly probe exciton dispersions in 2D semiconductors and could be generalized to many low-dimensional systems.

Two-dimensional (2D) transition metal dichalcogenides (TMDs) have shown great potential in applications for valleytronics [1-3] due to the indirect-to-direct bandgap crossover with drastically enhanced quantum efficiency. The opto-electronic applications of TMDs are often attributed to the optical response of electrons at the vicinity of K valley of the first Brillouin zone, inducing the so-called "valley excitons". However, most of the reported excitons in literature are excited at only zero-momentum transfer (q=0). The momentum (q) energy (E) dispersion of excitons is the key to understand the nature of the peculiar optical response in monolayer TMDs. Although recent theoretical calculations predict the q-E dispersions of valley excitons of monolayer TMDs[4-7], no reliable experiments have been performed to corroborate them.

There are several approaches to detect exciton dispersions of semiconductors, such as inelastic X-ray scattering, electron energy loss spectroscopy (EELS), or neutron scattering.

Inelastic X-ray/neutron scattering[8] is efficient to obtain the exciton dispersion but measures only bulk materials in millimeter size, and thus not capable for monolayer TMDs. On the other hand, reflection EELS requires a substrate for the sample, introducing non-negligible substrate-sample interaction. Hence, momentum (q) resolved EELS (q-EELS)[9,10] mostly in a transmission electron microscope (TEM) is a best choice to probe the intrinsic exciton dispersions of freestanding TMDs, as exemplified by the previous measurement of dispersions of plasmons in TMDs[11], graphene[12] and of phonons in h-BN[13,14]. In addition, TEM has superior spatial resolution to visualize the atomic structures of materials with possible local defects and impurities.

Here, taking advantage of the state-of-the-art energy/momentum resolution (ΔE~40meV, Δq=0.025Å^{-1}), we employ q-EELS to probe the q-E dispersions of various excitons in freestanding monolayer WSe_2 with prolific atomic defects. For the parabolically dispersed valley exciton A, non-dipole transitions play an increasingly prominent role as q increases, suggested by the oscillator strength evolution. Broad subgap exciton "x" was unexpectedly discovered at nonzero q and could be resulted from localized states caused by defects, lattice strain, and adsorbates, etc.

Experimental q-EEL spectra of freestanding monolayer WSe_2 were acquired in the standard diffraction mode in a TEM (JEOL-Triple C2) at 60 kV, as shown in Fig.1a. Spectra were taken in a Gatan spectrometer (GIF Quantum ER 965) from clean monolayer region of good crystalline quality (Fig. 1c and Fig.S1)[15]. With a monochromator, the energy resolution of 40~50 meV can be easily accessible (Fig.S2), quite necessary to distinguish exciton peaks (more elucidated in supplemental materials). In the diffraction space, we used a spectrometer entrance aperture (SEA) to select the specific in-plane momentum q along ΓM and ΓK directions (Fig.1b). The momentum resolution is defined by the size of SEA (1mm ~ 0.2mrad ~ 0.025Å^{-1}). In the following sections, the terminology "momentum q" always refers to in-plane momentum transfer, since the out-of-plane momentum can be neglected for our q range measured (Fig.S3). In real space, the spatial resolution is determined by the selected area aperture, which corresponds to an area of the monolayer in diameter ~200 nm. Figure 1d is a schematic illustration of electronic transitions from intrinsic band edges and localized electronic states, which results in valley exciton "A" and possible subgap exciton "x", which will be mentioned frequently later.

Figure 2 shows the q-E maps obtained along two typical in-plane orientations - ΓM and ΓK directions. For small momentum transfer q = 0~0.03 Å^{-1}, four branches of exciton peaks are clearly visible: A at 1.69 eV, B at 2.10 eV (here A, B peaks refer to the existing literatures) and

C at 2.50 eV, D at 3.00 eV (labeled as A′, B′ in other optical measurements[16,17]). The former two are often attributed to the intravalley excitons A_{1s} and B_{1s} from spin-splitting band-edge van Hove singularities[18] such as K_v-K_c transitions, and the latter peaks C, D from higher order Rydberg excited states like A_{2p} and B_{2p} (or A′, B′) [4,16,19]. Dispersive behaviours are unambiguously observed for the three branches of A, B, and C in Fig.2. As q increases, the three branches of excitons A, B, C present blueshifts with decreasing intensity but different dispersive curvatures. While the lowest-energy exciton A shows an everlasting intensity up to q = 0.2 Å^{-1}, the other excitons quickly disappear and get drowned into the background as q increases. It is worthwhile to mention that excitons can only survive in the range of q < 0.2 Å^{-1} in our experimental measurements. The exciton signal of monolayer WSe_2 for higher q is quite weak and undetectable with low signal-to-noise ratio.

The raw experimental q-EEL spectra are displayed in Fig.3 along ΓM and ΓK directions. Here we mainly consider excitons within the energy range ~ 4 eV of our interest. Higher energy excitation (5~8 eV) involves complicated exciton-plasmon interaction (Fig.S4 and Fig.S5) and their interpretations are not within the scope of this paper. As shown in Fig.3, the vertical dashed lines mark the position of all excitons A, B, C, D and E in the q→0 limit we observed. Above the well-known spin-splitting A, B excitons, the sharp C, D peaks are from Rydberg-state exciton A′ and B′ [4,16].

Along with the decreasing peak intensity, the blueshift of A exciton increases more and more obviously as q increases, indicating a nonlinear increasing dispersion. In the q-EELS in Fig.3, valley exciton A does not present obvious splitting as q increases. This is inconsistent with theoretical prediction of the splitting of the dispersion relations[4], maybe due to the limitation of energy resolution. Compared to sharp A exciton, the next three peaks B, C, D decrease and disappear synchronously on the background of the pre-tail of broad peak E which becomes dominating at q > 0.11 Å^{-1} (brown curve in Fig.3a). This background effect is more prominent when the thickness of WSe_2 increases (Fig. S6). In MoS_2, $MoSe_2$ and WS_2 system, the broad C peak due to band nesting has a much larger linewidth ΔE > 0.7 eV than the sharp A exciton with ΔE < 0.1 eV (ref. [19]) and this broad peak persists into high q (Fig.S7). Hence it is reasonable to assign the broad and intense peak E in WSe_2 as the electronic transition resulted from band nesting between Γ and Q point (Fig.1b)[18,20]. Strong excitonic effect accounts for the sharp and intense B, C, D exciton peaks before the broad peak E at q→0. However, a recent $k \cdot p$ model calculation[21] suggests that the broad E peak may also come from other van Hove singularities like the saddle point M (Fig.1b) in the optical band structure. Here it remains a controversial issue to unravel the origin of the most intense and broad postgap excitons in

TMDs. At lower energy end in Fig.3, we found a subgap exciton peak at 1.3 ~ 1.4 eV, as highlighted by the blue arrows and labeled as "*x*". The emergence of this "*x*" peak at nonzero *q* indicates its localization nature, exemplified by the atomic localization of phonons in h-BN at nonzero *q*[22]. This weak subgap feature can also be seen in Fig.2 and also in other TMDs in Fig.3c). This suggests that these common features in TMDs result from some unknown localized electronic states induced by defects, strain or surface adsorbates. Hence, further theoretical calculation of subgap localized excitons will be needed to understand the single photon emission whose origin remains controversial[23-26].

Profiling the peak positions of excitons using Voigt function fitting (Fig.S8), we derive their *q* dependence in Fig. 4. Here we focus only on A, E, and "*x*" excitons, as B,C,D excitons are on the pre-tail of E exciton and disappear too quickly. In Fig.4a, the measured *q*-*E* dispersions of A exciton show hardly any in-plane ΓM/ΓK anisotropy. Its dispersion can be well fitted by quadratic function, as expected from its valley exciton nature. Given that A exciton follows $E = \hbar^2 q^2/2m^*$, we can derive the effective mass of the A exciton $m^* = 0.65m_e$ (in Fig.4a), which agrees well with the GW calculated $0.72m_e$ in WSe_2 monolayer[5]. The value is also comparable with the effective mass of 3D traditional semiconductors.

To correlate with the quasiparticle band structure, we compare our results with theoretical dispersions derived from other band structure calculations, as shown in Fig.4b. In a simplified way (Fig.S9), exciton dispersion can be extracted from the electronic band structure: $E_g(q) = E_c(q) - E_v(0)$, where the initial state is fixed at K_v at $E_v(0)$ and final state at conduction band edge with momentum transfer *q* and energy $E_c(q)$. This simplified model has been employed in the case of bulk phosphorus of ref.[10]. More accurately, the initial state can be from any points nearby K_v, but with a momentum difference of *q* with respect to the final state on the conduction band edge. As shown in Fig.S9 and its caption, the parabolic dispersion approximation of valence/conduction bands still yields a parabolic exciton dispersion. Here, the A exciton dispersion are extracted from conduction band edge calculated by Wang et al[27], at the GW_0 level including spin-orbit coupling perturbatively. This GW_0 dispersion in Fig.4b presents a parabolic relation within the experimental *q* range we measured. In TMDs, the sharp A exciton peak at E_A is located below the threshold energy E_g (quasiparticle band gap) of the continuum absorption, and their difference is defined as exciton binding energy $E_b = E_g - E_A$ [4,27]. The experimental *q*-*E* relation is almost parallel with the GW_0-derived dispersion, and their difference means a binding energy E_b = 650 meV which is almost independent of *q*. This indicates the dispersion-less nature of exciton binding energy of 2D TMDs, also means the exciton radius remain almost unchanged in the Coulomb interaction for both *q*=0 and nonzero-*q*

excitations. Similarly, we derive the binding energy of B exciton as 760 meV. Compared to GW_0 dispersion, GW - Bethe Salpeter Equation (BSE) calculation[5] gives better accuracy in energy, but with a linear dispersion. The dispersion-less binding energy E_b~0.6-0.7eV, is much larger than that of traditional 3D semiconductors, as a result of less screening effect of the Coulomb interaction of excitons in freestanding monolayer TMDs. This also indicates the Frenkel nature of excitons in TMDs with a Bohr radius much smaller than nearly-free excitons in 3D GaAs, etc., implying a relatively lower charge carrier mobility.

Figure.4c shows the dispersion of the subgap exciton "*x*" and the broad peak E, beyond the range for accurate theoretical prediction. Out of one's expectation, the subgap exciton is quite dispersive with the increase of *q*. The right inset of Fig.4c shows the annular dark field scanning transmission electron microscopy (ADF-STEM) imaging of monolayer WSe_2. And the red circles highlight the most common defects - intrinsic Se vacancies, which may account for the subgap exciton "*x*". However, electronic transition from other localized states caused by lattice strain or surface adsorbates may also contribute to the appearance of sub-gap excitons. Here, we leave the origin of the subgap exciton as an open question of great interest calling for further theoretical/experimental exploration to unravel single photon emissions found in 2D materials. Furthermore, theoretical calculation of the *q* dependent absorption of atomic defects in 2D materials is drastically challenging, but helps to clarify the experimental findings. Compared to valley exciton A, exciton E presents a more complicated dispersion relation, shown in the left inset of Fig.4c. And it remains to be uncovered whether band nesting or van Hove singularity yields this broad and intense postgap E peak, as mentioned earlier.

Besides the exciton dispersion, the *q* dependence of the intensity of excitons often suggests the transition nature: dipole or multipole transition[28,29]. Among all excitons, we tracked the intensities of A and E excitons. As shown in Fig.5a, we compare the measured *q*-EELS intensity of A exciton with the GW-BSE[5] calculated and analytically-derived dipole approximation[28] results. Here, *q*-EELS, GW-BSE and dipole approximation present a decay of the intensity with the increase of momentum *q*. However, discrepancy appears in the decaying tail (marked by the arrows in Fig.5a) as *q* further increases > 0.08 $Å^{-1}$. The peak intensity of E presents a much slower decay than the dipole approximation at high *q*, shown in Fig. 5b. The discrepancy at high *q* imply the significant contribution of non-dipole, eg, quadrupole (Fig. 5b) or higher-order multipole transitions (Fig.S10)[28]. Here, the absence of data points as $q \rightarrow 0$ is to avoid the singularity in the scattering cross section (see Fig.S11). This non-dipole contribution may be responsible for the deviation of *q*-EELS/GW-BSE dispersions.

In contrast with dipole selection rule, quadruple momentum operator ($\boldsymbol{r}^2$) selects the initial and final states with the same parity. Here we simply use lowest unoccupied molecular orbitals (LUMO) and highest occupied molecular orbitals (HOMO) to interpret the possible origin of the dipole-multipole crossover as q increases. For A exciton, critical points K_v (d_{xy}, d_{x2-y2}) and K_c (d_{z2}) are both of even parity, and E exciton are of (d_{z2}, d_{xy}, d_{x2-y2}) orbitals[21]. Hence quadruple transition will get reasonably enhanced for both A and E excitons as in-plane momentum q increases.

Until now, we observe only $K_v \rightarrow K_c$ intravalley excitons (A,B,C,D) or other non-K transition (E) within a limited q (~0.2Å^{-1}). Recent GW-BSE calculation[5] of MX_2-TMDs (M=Mo,W; X=S,Se) predicts oscillator strength of excitons will also get maximized in high q range for $K_v \rightarrow Q_c$ and $K_v \rightarrow K_c'$ intervalley transitions. Therefore, the further measurements of the dispersions of intravalley and intervalley excitons by q-EELS would be of great interest. However, the experimental intensity for intervalley exciton is extremely low. Because inelastic scattering cross section decrease drastically at high q, and it is impossible to get a practical signal-to-noise ratio.

In summary, we used q-EELS in TEM to uncover the q-E dispersions of both valley and subgap excitons of monolayer WSe_2. The valley A exciton present a parabolic dispersion, and its binding energy of 0.65 eV is independent of momentum q. The oscillator strength evolution indicates the effects of non-dipole transition on A, E peak at large q, which may interpret the discrepancy of q-EELS/GW-BSE dispersions. In the future, improvement of the energy resolution (<10meV) and sandwiching by h-BN capping layer to form heterostructures may further facilitate in uncovering more fine structures of the dispersions of valley or subgap excitons. Our exploration of excitons in freestanding monolayer TMDs by q-EELS will inspire further theoretical/experimental research on subgap excitons resulted from localized states, which may offer hints to uncover the single photon emission in TMDs.

We acknowledge the support from JST Research Acceleration Programme and JSPS□KAKENHI (JP16H06333 and JP17H04797). We thank Dr. Quek Su Ying for help in the interpretation of experimental results and theoretical calculations.

References

[1] K. F. Mak, K. He, J. Shan, and T. F. Heinz, Nat. Nanotechnol. **7**, 494 (2012).
[2] H. Zeng, J. Dai, W. Yao, D. Xiao, and X. Cui, Nat. Nanotechnol. **7**, 490 (2012).
[3] T. Cao *et al.*, Nat. Commun. **3**, 887 (2012).
[4] D. Y. Qiu, T. Cao, and S. G. Louie, Phys. Rev. Lett. **115**, 176801 (2015).
[5] T. Deilmann and K. S. Thygesen, 2D Mater. **6**, 035003 (2019).
[6] H. Yu, G.-B. Liu, P. Gong, X. Xu, and W. Yao, Nat. Commun. **5**, 3876 (2014).

[7] P. Cudazzo, L. Sponza, C. Giorgetti, L. Reining, F. Sottile, and M. Gatti, Phys. Rev. Lett. **116**, 066803 (2016).
[8] H. Tornatzky, R. Gillen, H. Uchiyama, and J. Maultzsch, Phys. Rev. B **99**, 144309 (2019).
[9] R. Schuster, C. Habenicht, M. Ahmad, M. Knupfer, and B. Büchner, Phys. Rev. B **97**, 041201 (2018).
[10] R. Schuster, J. Trinckauf, C. Habenicht, M. Knupfer, and B. Büchner, Phys. Rev. Lett. **115**, 026404 (2015).
[11] R. Schuster, R. Kraus, M. Knupfer, H. Berger, and B. Büchner, Phys. Rev. B **79**, 045134 (2009).
[12] C. Kramberger *et al.*, Phys. Rev. Lett. **100**, 196803 (2008).
[13] F. S. Hage, R. J. Nicholls, J. R. Yates, D. G. McCulloch, T. C. Lovejoy, N. Dellby, O. L. Krivanek, K. Refson, and Q. M. Ramasse, Sci. Adv. **4**, eaar7495 (2018).
[14] R. Senga, K. Suenaga, P. Barone, S. Morishita, F. Mauri, and T. Pichler, Nature **573**, 247 (2019).
[15] See more details of methods and analysis in the supplemental material.
[16] W. Zhao, Z. Ghorannevis, L. Chu, M. Toh, C. Kloc, P.-H. Tan, and G. Eda, ACS Nano **7**, 791 (2013).
[17] A. Arora, M. Koperski, K. Nogajewski, J. Marcus, C. Faugeras, and M. Potemski, Nanoscale **7**, 10421 (2015).
[18] A. Carvalho, R. M. Ribeiro, and A. H. Castro Neto, Phys. Rev. B **88**, 115205 (2013).
[19] D. Kozawa *et al.*, Nat. Commun. **5**, 4543 (2014).
[20] M. Bieniek, M. Korkusiński, L. Szulakowska, P. Potasz, I. Ozfidan, and P. Hawrylak, Phys. Rev. B **97**, 085153 (2018).
[21] A. Kormányos, G. Burkard, M. Gmitra, J. Fabian, V. Zólyomi, N. D. Drummond, and V. Fal'ko, 2D Mater. **2**, 022001 (2015).
[22] F. Hage, D. Kepaptsoglou, Q. Ramasse, and L. Allen, Phys. Rev. Lett. **122**, 016103 (2019).
[23] Y.-M. He *et al.*, Nat. Nanotechnol. **10**, 497 (2015).
[24] M. Koperski, K. Nogajewski, A. Arora, V. Cherkez, P. Mallet, J.-Y. Veuillen, J. Marcus, P. Kossacki, and M. Potemski, Nat. Nanotechnol. **10**, 503 (2015).
[25] A. Srivastava, M. Sidler, A. V. Allain, D. S. Lembke, A. Kis, and A. Imamoğlu, Nat. Nanotechnol. **10**, 491 (2015).
[26] S. Zhang, C.-G. Wang, M.-Y. Li, D. Huang, L.-J. Li, W. Ji, and S. Wu, Phys. Rev. Lett. **119**, 046101 (2017).
[27] G. Wang, X. Marie, I. Gerber, T. Amand, D. Lagarde, L. Bouet, M. Vidal, A. Balocchi, and B. Urbaszek, Phys. Rev. Lett. **114**, 097403 (2015).
[28] M. Knupfer, T. Pichler, M. S. Golden, J. Fink, M. Murgia, R. H. Michel, R. Zamboni, and C. Taliani, Phys. Rev. Lett. **83**, 1443 (1999).
[29] A. V. Stier, N. P. Wilson, G. Clark, X. Xu, and S. A. Crooker, Nano Lett. **16**, 7054 (2016).
[30] T. C. Berkelbach, M. S. Hybertsen, and D. R. Reichman, Phys. Rev. B **88**, 045318 (2013).

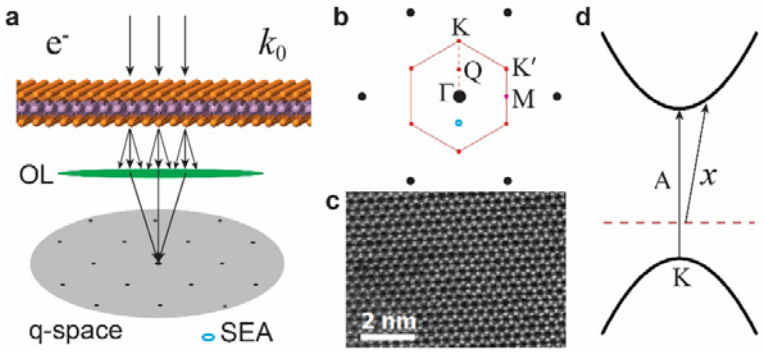

FIG. 1. Scattering geometry for *q*-EELS. (a) *q* space in parallel-beam electron diffraction. The momentum resolution is determined by the post-screen spectrometer entrance aperture (SEA). (b) First Brillouin zone critical points in the diffraction pattern, where the blue circle stands for SEA and selects the specific *q*. (c) Atomically resolved annular dark field scanning transmission electron microscopy (ADF-STEM) image of freestanding monolayer WSe_2. (d) Schematic illustration of intrinsic band edges at K point and localized electronic states within the gap, which yield $K_v \rightarrow K_c$ valley exciton "A" and subgap exciton "*x*".

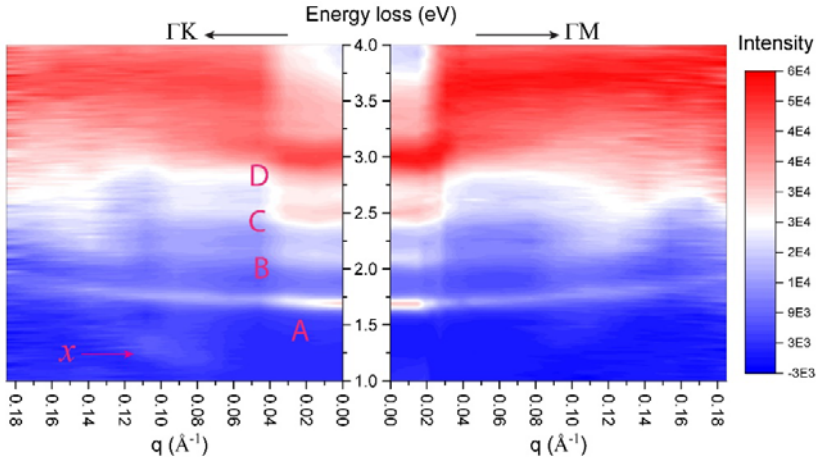

FIG. 2. Experimental *q*-*E* diagram of freestanding monolayer WSe_2. The *q*-serial low loss spectra were acquired along ΓK and ΓM directions, respectively. Dispersive bands can be observed: A exciton at 1.70 eV, B exciton at 2.1 eV, and C exciton at 2.5 eV.

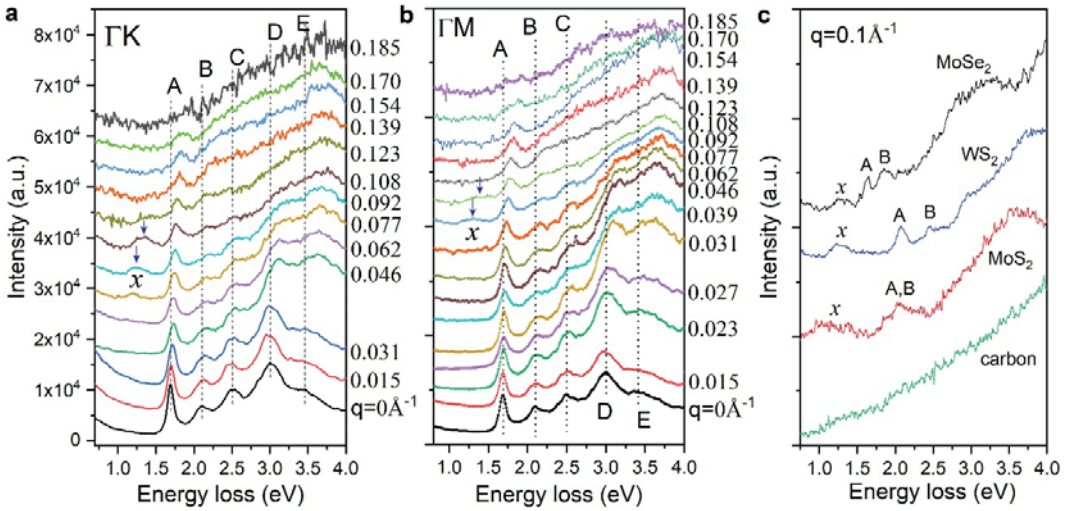

FIG. 3. The *q*-EEL spectra fine structures of WSe_2 along ΓK (a) and ΓM (b) directions. Dashed lines mark the exciton peaks (A, B, C, D, E) at q=0 and guide eyes for the blue-shifting. Besides these major features, a subgap exciton "*x*" at 1.4 eV emerges and gets enhanced at q = 0.1 $Å^{-1}$, highlighted by blue arrows. (c) The low loss spectra of different materials at intermediate q=0.1$Å^{-1}$. The sub-gap signal "*x*" appears in all TMDs at nonzero q only, indicating this material dependent feature is localized in real space.

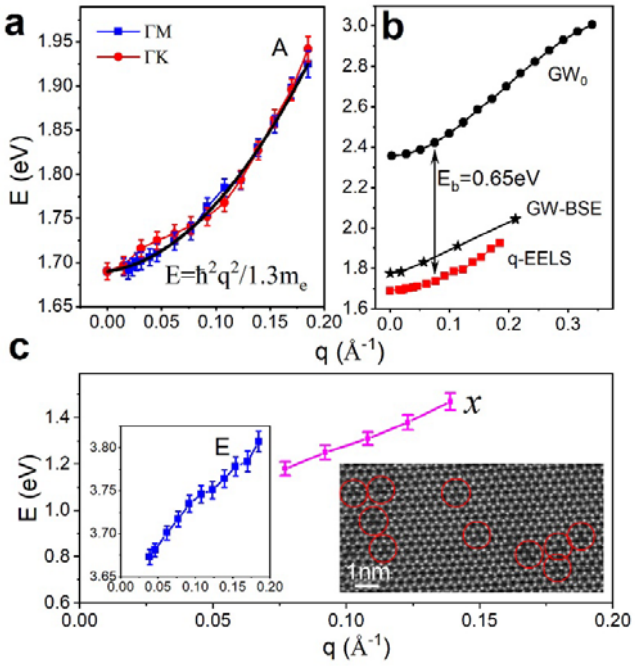

FIG. 4. Exciton dispersions. (a) The extracted q dependence of A exciton energy. No obvious in-plane anisotropy for ΓM and ΓK is observed. (b) A comparison of A exciton dispersions by q-EELS and other theoretical calculations. GW_0 data is extracted from electronic band structure by Wang et al.[27] (Fig.S9) and GW-BSE by Deilmann et al.[5]. (c) Dispersion of the subgap exciton "x", possibly resulted from rich Se vacancies shown in the right inset. The left inset shows exciton E has a complicated dispersion behavior.

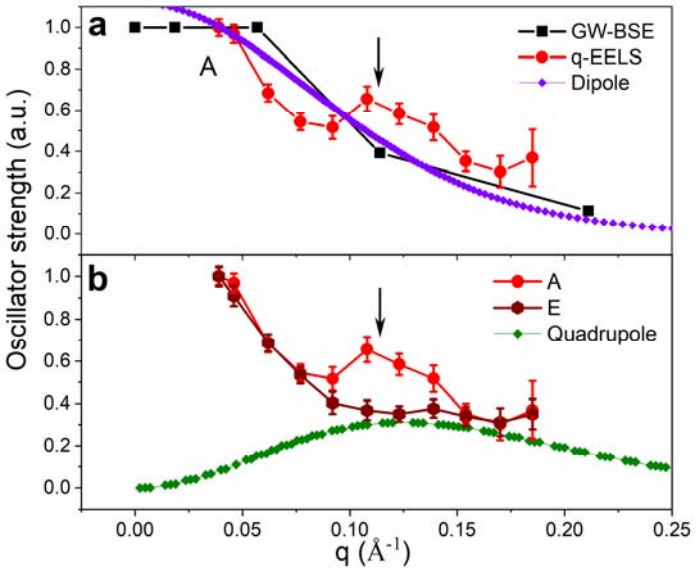

FIG. 5. The q dependence of exciton peak intensity. (a) The q dependence of A excitons. The GW-BSE intensity evolution in black is extracted from the calculation by Deilmann et al[5]. The curve in purple is from dipole approximation (analytical) of the transition matrix element by Knupfer et al[28], where the Bohr radius of A exciton is set as 17 Å (close to the report 10 ~ 20 Å by Stier et al[29] and Berkelbach et al[30]). The black arrow indicates the discrepancy of the decaying tail of the experimental and theoretical q distributions. (b) The q dependence of oscillator strength of A and E peaks and theoretical quadruple contribution. The quadruple contribution may well interpret the discrepancies of the decaying tails.